Stochastic Oscillation in Self-Organized Critical States of Small Systems: Sensitive Resting State in Neural Systems

Sheng-Jun Wang,[1,2] Guang Ouyang,[2] Jing Guang,[3] Mingsha Zhang,[3,*]
K. Y. Michael Wong,[4] and Changsong Zhou[2,5,6,†]

[1]*Department of Physics, Shaanxi Normal University, Xi'An 710119, China*
[2]*Department of Physics, Centre for Nonlinear Studies and Beijing-Hong Kong-Singapore Joint Centre for Nonlinear and Complex Systems (Hong Kong), Institute of Computational and Theoretical Studies, Hong Kong Baptist University, Kowloon Tong, Hong Kong*
[3]*State Key Laboratory of Cognitive Neuroscience and Learning, Beijing Normal University, Beijing 100875, China*
[4]*Department of Physics, Hong Kong University of Science and Technology, Clear Water Bay, Hong Kong*
[5]*Beijing Computational Science Research Center, Beijing 100084, China*
[6]*Research Centre, HKBU Institute of Research and Continuing Education, Virtual University Park Building, South Area Hi-tech Industrial Park, Shenzhen 518057, China*

(Received 23 December 2014; revised manuscript received 15 November 2015; published 8 January 2016)

Self-organized critical states (SOCs) and stochastic oscillations (SOs) are simultaneously observed in neural systems, which appears to be theoretically contradictory since SOCs are characterized by scale-free avalanche sizes but oscillations indicate typical scales. Here, we show that SOs can emerge in SOCs of small size systems due to temporal correlation between large avalanches at the finite-size cutoff, resulting from the accumulation-release process in SOCs. In contrast, the critical branching process without accumulation-release dynamics cannot exhibit oscillations. The reconciliation of SOCs and SOs is demonstrated both in the sandpile model and robustly in biologically plausible neuronal networks. The oscillations can be suppressed if external inputs eliminate the prominent slow accumulation process, providing a potential explanation of the widely studied Berger effect or event-related desynchronization in neural response. The features of neural oscillations and suppression are confirmed during task processing in monkey eye-movement experiments. Our results suggest that finite-size, columnar neural circuits may play an important role in generating neural oscillations around the critical states, potentially enabling functional advantages of both SOCs and oscillations for sensitive response to transient stimuli.

DOI: 10.1103/PhysRevLett.116.018101

Self-organized criticality [1] is a key concept for describing the emergence of complexity in many natural systems [2]. The fingerprint of self-organized critical states (SOCs), the power-law distribution of avalanche sizes, means that the activity has no characteristic scale in the thermodynamic limit. As excellent functional complex systems in nature, neural systems in the brain have been supposed to operate at SOCs. Indeed, SOCs of neuronal firing activity have been observed in experiments with electrode arrays [2–4] and have been studied intensively in computational models [2,5,6]. It has been shown that critical states have functional advantages for both the sensory system [7] and memory [8], and they play an important role in the development of neural systems [9].

On the other hand, stochastic oscillation (SO) in brain activity has been observed for more than 80 years [10]. Oscillations characterized by repetition of activities with typical scales are believed to be essential to brain functions, especially to provide timing, predictability, coherence, and integration in neural information processing [11]. Several different oscillation bands exist and appear in different states of the brain [10]. The synchronization between inhibitory neurons has been found to be crucial for gamma oscillations (30–70 Hz) [12]. Neural field models [13] indicated that resonance between thalamus and cortex can generate alpha oscillations (8–13 Hz). Despite many modeling studies, a commonly accepted mechanism of alpha rhythm is still lacking [14]. This slow oscillation is particularly obvious during the resting states without systematic external stimuli (i.e., eyes closed). It has been known through the *Berger effect*, or *alpha blockade*, for a long time that when observers open their eyes, the electroencephalography (EEG) alpha oscillations decrease in amplitude or disappear completely [15]. Such oscillations can also be suppressed during cognitive task processing, typically known as event-related desynchronization (ERD) [16], apparently suggesting that alpha oscillations and suppression are due to synchronization and desynchronization processes. ERD has been widely used as a sensitive measure for brain-computer interfaces (see a review in Ref. [17]).

SOCs and SOs of neural systems are often studied in different models with the implicit assumption that different activities do not coexist [18]. However, experiments on

SOCs of neural activity actually also showed pronounced oscillations of local field potentials (LFPs) [3,18], and the coexistence of them has been explicitly analyzed in the maturation of the cortex [19]. Modeling studies found that they can indeed coexist in biologically plausible neuronal networks [20,21]. These studies raised an important theoretical question: how could the apparently contradictory scale-free SOCs and scale-typical oscillations coexist?

Though neural systems in the brain contain a huge number of neurons, finite-size effects could be important due to very prominent hierarchical modular structures [22]. Local neuronal circuits are characterized by minicolumns composed of a few hundred neurons clustered in space and densely connected [22]. Such inherently modular organization inspired us to study in this Letter the role of finite-size effects on the reconciliation of SOCs and SOs. We propose that finite-size effects of SOC can generically induce the oscillation features which can be robustly observed in biologically plausible neural network models and can explain the Berger effect. The generic features of the model are confirmed in experiments in waking monkeys. Our work suggests new anatomical and dynamical mechanisms of oscillations in the brain that have not been investigated previously.

We first use the prototype sandpile model [1] to study the oscillation property of SOCs. On a 2D lattice of size $N = L \times L$, when the amount of sand $z(x, y)$ exceeds a threshold K, $z(x, y)$ is subtracted by 4 and each neighbor of (x, y) is increased by 1 or drops out at the boundary. At each time step, if no vertex exceeds K, a site (x, y) is randomly selected and $z(x, y)$ is increased by a small constant value Δz. To study the effect of external driving, we set $\Delta z \leq 1.0$, different from previous studies fixed at 1.0. We study the temporal properties of the number of superthreshold sites N_s. Avalanches occur under weak perturbation [see Fig. 1(a), left and right segments]. Strong stimuli drive the system into a persistent noisy response [see Fig. 1(a), middle segment].

There is a broad peak in the power spectrum [see Fig. 1(b)] of N_s under weak stimuli, suggesting that SO is exhibited by the SOC state of the sandpile model [see the Fig. 1(b) inset for the power-law distribution of avalanche sizes with cutoff]. The peak frequency becomes smaller for larger system sizes [see Fig. 1(c)] and is larger with stronger stimulus strength Δz [Fig. 1(d); see Fig. S1 for size distributions and spectra in Supplemental Material I [23]]. This is different from previous work ($N = 20^3$) [25], where the power spectrum from short time series was considered and the low frequency part is flat as white noise. A stable peak appears only for long enough time series which can capture slow oscillations (see Figs. S2 and S3, Supplemental Material II [23]).

However, we emphasize that this rhythm is a feature of *self-organized* criticality rather than critical states without self-organized processes. SOCs require a slow driving to gradually build up the sandpile, which is released when a certain threshold is overcome. This accumulation-release process is an essential property of SOCs. As a comparison, the temporal property of the critical branching process is studied. Though used to understand the power-law distribution of avalanche size in SOCs [26,27], the critical state in the branching process is set by a control parameter rather than achieved by a self-organized process, and it does not display oscillations. Oscillations in the sandpile model are eliminated if the avalanches are shuffled in time, while keeping the same distributions with finite-size cutoff (see Fig. S4 in Supplemental Material III [23]).

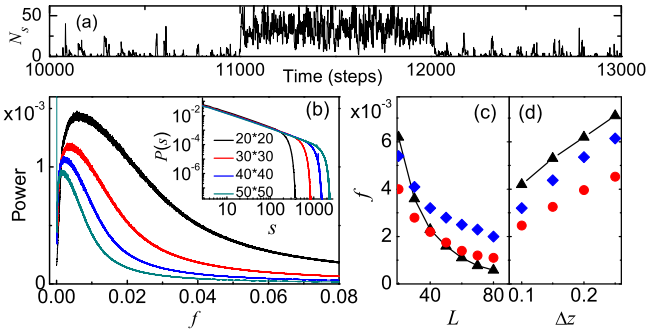

FIG. 1. (a) Time series of the number of superthreshold sites N_s. For the left and right segments, one site is added by $\Delta z = 0.2$; for the middle segment, ten sites are added by 1.0 at each step. (b) Power spectrum density (PSD) of N_s for various lattice sizes. The length of time series is 2^{18}. (Inset) The power-law distribution of avalanche sizes. Dependence of the peak frequency (the triangles) on lattice width L (c) and stimulus strength Δz (d). The circles and diamonds are the frequency values obtained by Eqs. (1) and (2), respectively.

Let us first present a qualitative interpretation of the SO exhibited in SOCs. As a result of the accumulation-release process, in a small system, there is no large avalanche immediately after a large avalanche similar to the system size. It takes a typical period of time to accumulate before another large release close to the system size occurs, leading to stochastic periodicity of large avalanches and SO in the time series. The period becomes longer for larger system size L or smaller stimulus strength Δz since it takes longer time to accumulate. Between large avalanches, the small avalanches are more random because it depends on where the stimulus is added. So there are no significant correlations between small avalanches, and noise dominates the power spectrum at high frequency. In the thermodynamic limit, no systematic correlation can be established and the oscillations disappear.

The following quantitative analysis verifies the interpretation. We divide avalanches into different nonoverlapping ranks using the average duration $d(s)$ for avalanches of size s, as illustrated in Fig. 2(a) (see the details in Supplemental Material IV [23]), and we analyze the time series of the avalanches of a given rank by removing all of the other avalanches. There is a peak in the power spectrum

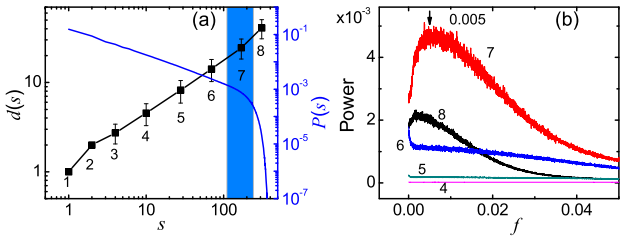

FIG. 2. (a) Illustration of classification of avalanches. The blue solid line is the avalanche size distribution. The shaded bar highlights the avalanche rank at the crossover to cutoff. (b) PSD of each rank of avalanches. Lattice size is $N = 20 \times 20$.

of the time series of large avalanches, e.g., for ranks 7 and 8, but no peak for small avalanches [see Fig. 2(b)]. Avalanches at the crossover to the cutoff (rank 7) contribute most significantly to the power spectrum of the SOCs since such large avalanches still have a high probability of occurring. The frequency of rank r can be estimated as the rate for finding avalanches of the rank

$$f(r) = \left[n \sum_{s \in r} P(s)\right] \Big/ T, \tag{1}$$

among the total number of avalanches n in all ranks in a long time period T. Indeed, $f(r)$ for the crossover rank can give a good account for the dependence of the peak frequency on N and Δz [see Figs. 1(c) and 1(d), circles].

Then we proceed to estimate the frequency using the accumulation-release dynamics. A period T_g is finished by a giant avalanche with size $s \in [s_1, N]$. The total input minus the leaking of small avalanches equals the leaking of the giant avalanche. The equation is

$$\Delta z(T_g - T_d) - \int_1^{s_1} l(s)P(s)N_a ds = \int_{s_1}^{N} l(s)P(s)N_a ds, \tag{2}$$

where N_a is the number of avalanches in the period, $N_a \int_{s_1}^{N} P(s)ds = 1$. T_d is the total duration of avalanches before the giant one, $T_d = \int_1^{s_1} d(s)P(s)N_a ds$. $d(s)$ and $l(s)$ are the mean duration and leaking of avalanches with size s. We take the value of s_1 as the lower boundary of crossover rank in the avalanche size distribution $P(s)$ [e.g., rank 7 in Fig. 2(a)]. The frequency $f = 1/T_g$ is obtained by numerically solving Eq. (2) using the $P(s)$, $d(s)$, and $l(s)$ obtained in simulations. Although the crossover threshold s_1 is only heuristically determined, the frequency estimated from the accumulation-release process follows the same trend of size dependence [see Fig. 1(c)]. Equation (2) also explains that a larger driving Δz increases the frequency [see Fig. 1(d), diamonds], although the avalanche size distributions are very similar for weak stimuli (see Fig. S1).

Now we show that SOs in SOCs can exist in a biologically plausible neural network model with excitation-inhibition (E-I) balance. E-I balance has been demonstrated experimentally [28]. To mimic the modules of local cortical networks, we analyze an isolated, small, and dense random network (connectivity $p = 0.16$; 80% of excitatory neurons) with weak background input. The dynamics of neurons reads [29,30]

$$\tau \frac{dV}{dt} = (V_{\text{rest}} - V) + g_{\text{ex}}(E_{\text{ex}} - V) + g_{\text{inh}}(E_{\text{inh}} - V). \tag{3}$$

When the membrane potential V crosses a threshold (-50 mV), the neuron fires a spike. Then V is reset to $V_{\text{rest}} = -60$ mV and fixed for a refractory period (5 ms). The spike of excitatory (or inhibitory) neuron increases the synaptic conductance of postsynaptic targets by Δg_{ex} (or Δg_{inh}), which decay exponentially with time constant τ_{ex} (or τ_{inh}). The biological values of parameters [30] are $\tau = 20$ ms, $E_{\text{ex}} = 0$ mV, $E_{\text{inh}} = -80$ mV, $\tau_{\text{ex}} = 5$ ms, and $\tau_{\text{inh}} = 10$ ms. Each neuron receives an independent external excitatory Poisson spike train with rate η. The neural network transits from silent (order) to sustained (disorder) activity when the excitatory coupling strength increases [20]. The continuous phase transition between order and disorder of neural networks was demonstrated in the small perturbation limit [31]. The dissipation properties from the leaking of membrane, refractory period, and, most importantly, inhibitory neurons make the neural network model much more complicated than the sandpile one.

In simulations, we obtained the coexistence of SOCs and SOs [see Figs. 3(a) and 3(b)]. The avalanche size measured by the number of spiking neurons during an avalanche is distributed by power law [the circles in Fig. 3(c)]. The

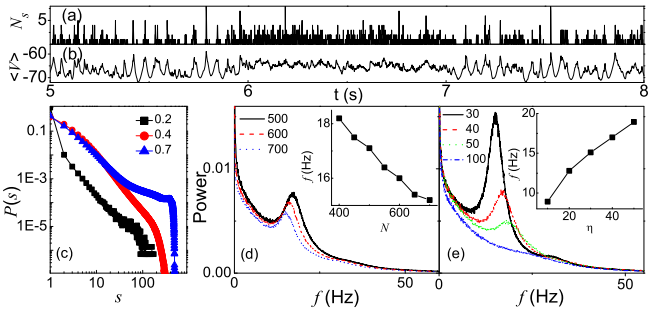

FIG. 3. (a) The population activity N_s and (b) the mean membrane potential $\langle V \rangle$ of the network in the critical regime with weak background input $\eta = 40$ Hz and additional strong stimulus $\eta = 400$ Hz in Refs. [6,7]. (c) Distribution of avalanche size $P(s)$ for the critical (circles), subcritical (squares), and supercritical (triangles) regimes. (d),(e) PSD of $\langle V \rangle$ in the critical regime for various networks of size N and input rate η. (Inset) The peak frequency. The parameters in (a),(b),(d),(e) are $\Delta g_{\text{ex}} = 0.4$, $\Delta g_{\text{inh}} = 4.0$.

subcritical and supercritical distributions were also plotted [the squares and triangles in Fig. 3(c)]. Interestingly, a pronounced peak is shown at low frequency on the power spectrum of $\langle V \rangle$ [see Fig. 3(d)]. It is consistent with the characteristics of alpha EEG of a resting human brain [10], where a peak is overlapped on a noisy background. Similar to the sandpile model, the oscillation frequency decreases with network size and increases with stimulus strength [the insets of Figs. 3(d) and 3(e); see the size distributions in Fig. S6 of Supplemental Material V [23]). A detailed comparison of the spectra shows that the much more complicated neural network model displays generic features of the sandpile model (Supplemental Material VI [23]).

An essential property of SOCs is that they require weak external driving [see Fig. 1(a)]. It was observed *in vivo* that SOCs are depressed by large stimuli [32]. Figure 3(e) shows that pronounced oscillations disappear when stimuli are strong enough (the blue line at $\eta = 100$ Hz). This property of SOCs provides a potential mechanism for the Berger effect. The slow oscillations disappear when a high rate stimulus ($\eta = 400$ Hz) is present and recover when the stimulus is removed [see Fig. 3(b)], which closely reproduces the Berger effect [15].

The co-organization of SOCs and SOs occurs in a broad region of the parameters (Δg_{ex}, Δg_{inh}) (see Fig. 4). While excitatory neural networks need a fine-tuned strength to achieve the criticality [33], activity dependent depression [5,34], here from inhibitory neurons, allows the criticality to organize in a wide region. The critical region [the blue region in Fig. 4(a)] broadly overlaps with the region of oscillation with only one pronounced peak at the main frequency [see Fig. 4(b)]. In subcritical states there is no peak, while in supercritical states multiple peaks appear [see the inset of Fig. 4(b)]. Previously, neural oscillations were explained by the alternating activation between excitatory and inhibitory populations (the E-I loop) [35]. In our model oscillations can also emerge due to the accumulation-release process in small systems at SOCs, where the quick release activates the E-I loop. The E-I loop becomes dominant in supercritical states without a pronounced accumulation interval (see Supplemental Material VII [23], Fig. S10).

The co-organization of SOCs and SOs enables the system to display responsiveness of both SOCs and oscillations. Critical states can respond sensitively, as shown in Fig. 5(a), where transient stimuli of different durations with $\eta_1 = 50$ Hz are added on the background driving ($\eta = 20$ Hz). With the background stimuli, the average firing rate of neurons is $r = 4.5$ Hz. The firing rate increases clearly at the critical region, similar to critical states in the network of excitatory elements [7]. Meanwhile, due to oscillation, the response of the SOCs can display "phase sensitivity" [see Fig. 5(b)], where the phase depends on $\langle V \rangle$ [see Fig. 3(b)] at the onset of the stimuli. The finite size causes the network to stay away from criticality after a large avalanche, and accumulation brings it back again (see Supplemental Material XIII [23]), and response is strongest for $\langle V \rangle \sim -60$ mV after the accumulation. Such self-organized temporal oscillations around the criticality provide the system with a new dimension of manipulation of the highly sensitive criticality for information processing. Dependence of the stimulus-driven activation on the phases of ongoing brain waves has been observed in cognitive experiments [36].

Using LFP recordings from an array of electrodes, the existence of SOCs in cortical networks has been extensively demonstrated in experiments [2–4]. Here, we confirm the features of response of neural oscillations using LFP data from an *in vivo* experiment on a monkey during saccadic eye movements [37]. Only one electrode is used to record the LFP before target onset, during and after task processing in the lateral intraparietal (LIP) area of the monkey, since the LIP area is folded strongly; see Supplemental Material IX [23] for more details. Figure 6 shows clearly that slow waves are predominant in the alpha band (~12 Hz) before the target onset. The LFP fluctuates strongly [see Fig. 6(a), upper panel], though a single electrode does not capture the spreading of large avalanches. During the task processing, the multiunit spiking

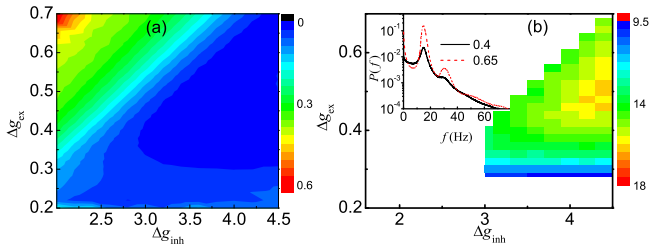

FIG. 4. (a) The deviation of the avalanche size distribution from the best-fitting power law [5]. (b) The parameter region where oscillations can exhibit a single peak in PSD. Color represents the peak frequency. (Inset) PSD for subcritical ($\Delta g_{ex} = 0.21$), critical ($\Delta g_{ex} = 0.4$) and supercritical ($\Delta g_{ex} = 0.65$) states of the neural network with $\Delta g_{inh} = 4.0$ and $N = 500$.

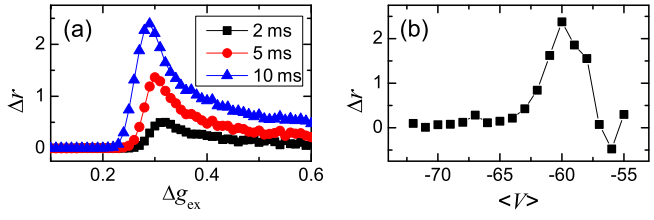

FIG. 5. Phase-sensitive response of critical oscillations to weak transient stimuli. (a) The stimulus-increased firing rate Δr versus Δg_{ex}. The stimuli last for 2, 5, and 10 ms. The firing rate is computed over a window (50 ms) after the stimulation. (b) The response of critical states versus the mean membrane potential at the timing of adding stimuli (lasting for 1 ms). Here, $\Delta g_{inh} = 4.0$ and $N = 500$.

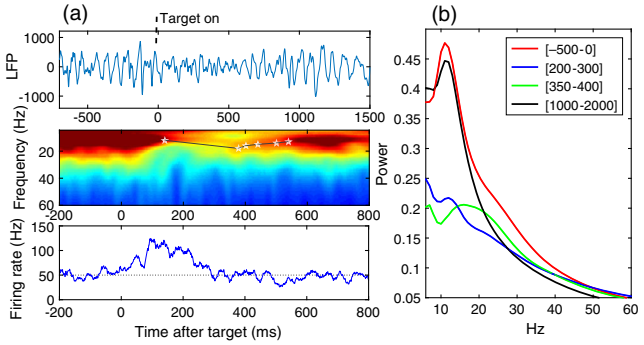

FIG. 6. (a) The local field potential (LFP) obtained in an experiment (upper panel, typical single experimental trial) and the time-frequency plot (middle panel, wavelet, peak marked by stars) and the multiunit spiking rate (baseline indicated by the dashed line), averaged over 50 trials. (b) Averaged PSD for the waves at rest (−550 − 0 ms) and during (200–300 ms and 350–400 ms) and after (1000–2000 ms) task processing.

rate increases from the prestimulus baseline and then recovers [see Fig. 6(a), bottom panel]. Correspondingly, the slow oscillations are almost fully suppressed (e.g., [200–300] ms) and then recover with higher peak frequency (e.g., ∼20 Hz in [350–400] ms). The oscillations are largely restored quickly after the task processing [see Fig. 6(b)]. The behavior of LFP agrees with the Berger effect and event-related desynchronization [16]. The response features are closely consistent with the generic model [see Fig. 3(e)].

Similar suppression of alpha oscillations is robustly observed at another recording site together with a pronounced gamma rhythm [see Fig. S11 of Supplemental Material IX [23]). The main qualitative features in Figs. 6 and S11 can be simultaneously reproduced in our generic models assuming a transient input to the local circuit, considering fast-spiking interneurons [12,38] (Figs. S14 and S15; see Supplemental Material X [23]).

In summary, we showed that SOCs generically exhibit rhythm on small systems due to the accumulation-release process. For neural systems, the finite-size effect could indeed be significant due to the modular structure of cortical circuits. The generic features of neural oscillations and response to stimulations in the excitation-inhibition balanced model were simultaneously confirmed by an *in vivo* experiment, suggesting an accumulation-release process in the local circuit as the dynamical mechanism underlying the Berger effects or event-related desynchronization, but not necessarily synchronization and desynchronization. The co-organization of oscillations and critical states would allow the system to take advantage of a sensitive response to weak signals in SOCs and a phase-dependent response in oscillations for efficient information processing.

This work was partially supported by Hong Kong Baptist University Strategic Development Fund, NSFC-RGC Joint Research Scheme HKUST/NSFC/12-13/01 (or N-HKUST 606/12), RGC (Grants No. 604512, No. 605813, and No. 12302914), NSFC (Grants No. 11275027, No. 11328501, and No. 11305098), and the Fundamental Research Funds for the Central Universities (Grant No. GK201302008).

*mingsha.zhang@bnu.edu.cn
†cszhou@hkbu.edu.hk

[1] P. Bak, C. Tang, and K. Wiesenfeld, Phys. Rev. Lett. **59**, 381 (1987).
[2] D. Plenz and H. G. Schuster, *Criticality in Neural Systems* (Wiley, New York, 2014).
[3] J. Beggs and D. Plenz, J. Neurosci. **23**, 11167 (2003); **24**, 5216 (2004).
[4] T. Petermann, T. C. Thiagarajan, M. A. Lebedev, M. A. Nicolelis, D. R. Chialvo, and D. Plenz, Proc. Natl. Acad. Sci. U.S.A. **106**, 15921 (2009); G. Hahn, T. Petermann, M. N. Havenith, S. Yu, W. Singer, D. Plenz, and D. Nikolic, J. Neurophysiol. **104**, 3312 (2010); G. Scott, E. D. Fagerholm, H. Mutoh, R. Leech, D. J. Sharp, W. L. Shew, and T. Knöpfel, J. Neurosci. **34**, 16611 (2014).
[5] A. Levina, J. M. Herrmann, and T. Geisel, Nat. Phys. **3**, 857 (2007).
[6] L. de Arcangelis, C. Perrone-Capano, and H. J. Herrmann, Phys. Rev. Lett. **96**, 028107 (2006); D. Millman, S. Mihalas, A. Kirkwood, and E. Niebur, Nat. Phys. **6**, 801 (2010); S. Wang and C. Zhou, New J. Phys. **14**, 023005 (2012).
[7] O. Kinouchi and M. Copelli, Nat. Phys. **2**, 348 (2006).
[8] C. Haldeman and J. M. Beggs, Phys. Rev. Lett. **94**, 058101 (2005).
[9] C. V. Stewart and D. Plenz, J. Neurosci. **26**, 8148 (2006); M. Hennig, C. Adams, D. Willshaw, and E. Sernagor, *ibid.* **29**, 1077 (2009).
[10] G. Buzsáki, *Rhythms of the Brain* (Oxford University Press, New York, 2006).
[11] G. Buzsáki and A. Draguhn, Science **304**, 1926 (2004).
[12] J. Cardin, M. Carlén, K. Meletis, U. Knoblich, F. Zhang, K. Deisseroth, L. Tsai, and C. Moore, Nature (London) **459**, 663 (2009); X. Wang and G. Buzsáki, J. Neurosci. **16**, 6402 (1996).
[13] P. A. Robinson, C. J. Rennie, and D. L. Rowe, Phys. Rev. E **65**, 041924 (2002).
[14] J. Shaw, *The Brain's Alpha Rhythms and the Mind* (Elsevier, New York, 2003).
[15] K. Kirschfeld, Biol. Cybern. **92**, 177 (2005).
[16] G. Pfurtscheller, Electroencephalogr. Clin. Neurophysiol. **43**, 757 (1977); W. Klimesch, M. Doppelmayr, T. Pachinger, and H. Russegger, Cognit. Brain Res. **6**, 83 (1997); W. Klimesch, Trends Cognit. Sci. **16**, 606 (2012).
[17] G. Pfurtscheller and C. Neuper, Prog. Brain Res. **159**, 433 (2006).
[18] J. Hesse and T. Gross, Front. Syst. Neurosci. **8**, 166 (2014).
[19] E. Gireesh and D. Plenz, Proc. Natl. Acad. Sci. U.S.A. **105**, 7576 (2008).

[20] S. Wang, C. Hilgetag, and C. Zhou, Front. Comput. Neurosci. **5**, 30 (2011).
[21] S. Poil, R. Hardstone, H. Mansvelder, and K. Linkenkaer-Hansen, J. Neurosci. **32**, 9817 (2012).
[22] V. Mountcastle, Brain **120**, 701 (1997); D. P. Buxhoeveden and M. F. Casanova, *ibid.* **125**, 935 (2002); C. Hilgetag, G. Burns, M. O'Neill, J. Scannell, and M. Young, Phil. Trans. R. Soc. B **355**, 91 (2000); C. Hilgetag and M. Kaiser, Neuroinformatics **2**, 353 (2004).
[23] See Supplemental Material at http://link.aps.org/supplemental/10.1103/PhysRevLett.116.018101, which includes Ref. [24], for details.
[24] D. B. Larremore, W. L. Shew, and J. G. Restrepo, Phys. Rev. Lett. **106**, 058101 (2011).
[25] P. Bak, C. Tang, and K. Wiesenfeld, Phys. Rev. A **38**, 364 (1988).
[26] P. Alstrøm, Phys. Rev. A **38**, 4905 (1988).
[27] W. L. Shew, H. Yang, T. Petermann, R. Roy, and D. Plenz, J. Neurosci. **29**, 15595 (2009); W. L. Shew, H. Yang, S. Yu, R. Roy, and D. Plenz, *ibid.* **31**, 55 (2011).
[28] Y. Shu, A. Hasenstaub, and D. A. McCormick, Nature (London) **423**, 288 (2003); A. Renart, J. de la Rocha, P. Bartho, L. Hollender, N. Parga, A. Reyes, and K. D. Harris, Science **327**, 587 (2010).
[29] C. Vreeswijk and H. Sompolinsky, Science **274**, 1724 (1996).
[30] T. P. Vogels and L. F. Abbott, J. Neurosci. **25**, 10786 (2005).
[31] R. V. Williams-García, M. Moore, J. M. Beggs, and G. Ortiz, Phys. Rev. E **90**, 062714 (2014).
[32] V. Priesemann, M. Wibral, M. Valderrama, R. Pröpper, M. Le Van Quyen, T. Geisel, J. Triesch, D. Nikolić, and M. H. J. Munk, Front. Syst. Neurosci. **8**, 108 (2014).
[33] C. W. Eurich, J. M. Herrmann, and U. Ernst, Phys. Rev. E **66**, 066137 (2002).
[34] J. Tabak, W. Senn, M. J. O'Donovan, and J. Rinzel, J. Neurosci. **20**, 3041 (2000).
[35] N. Brunel and X. Wang, J. Neurophysiol. **90**, 415 (2003).
[36] K. Linkenkaer-Hansen, V. V. Nikulin, S. Palva, R. J. Ilmoniemi, and J. M. Palva, J. Neurosci. **24**, 10186 (2004); K. E. Mathewson, G. Gratton, M. Fabiani, D. M. Beck, and T. Ro, *ibid.* **29**, 2725 (2009); T. P. Zanto, J. Z. Chadick, and A. Gazzaley, NeuroImage **85**, 794 (2014).
[37] M. Chen, Y. Liu, L. Wei, and M. Zhang, J. Neurosci. **33**, 814 (2013).
[38] E. M. Izhikevich and G. M. Edelman, Proc. Natl. Acad. Sci. U.S.A. **105**, 3593 (2008).